Aerodynamics and Aeroacoustics Optimization of Rotor Blade in Hover

Yufan Bi[2], Xu Zhao[1,2], Haiyang Yu[2], Linyan Huang[2]

[1]*National Key Laboratory of Science and Technology on Aerodynamic Design and Research，Northwestern Polytechnical University, Xi'an, Shaanxi, 710072, China*
[2]*School of Aeronautics, Northwestern Polytechnical University, Xi'an, Shaanxi, 710072, China*

Abstract. The design of silent and high-performance rotors is currently one of the development directions of helicopter technology. To achieve this goal, this paper effectively integrates multi-modules of rotor aerodynamics and aeroacoustics, presenting a Multidisciplinary Design Optimization (MDO) process for designing a quiet and efficient helicopter blade in hover.

The original blade configuration is selected with a double-swept and anhedral blade tip at working condition of rotational speed 1300 rpm. The swept position, swept angle, anhedral angle, twist angle, collective pitch, chord length and taper ratio of the blade are set as optimization parameters. The figure of merit and the Overall Sound Pressure Level (OASPL) at rotating plane are chosen as optimization objectives. A program is developed for parameterized modeling of blade and automatic generation of unstructured grids. The aerodynamic performance of the blade is predicted by CFD models to discretize RANS equation on a quasi-steady flow model and an unsteady flow model. Meanwhile, the sound field simulation of the blade is performed by using Ffowcs Williams-Hawkings (FW-H) equation on the above flow field calculations considering thickness and load noise for the quasi-steady model and including blade tip and wake noise as well for the unsteady model. The aerodynamic and aeroacoustics results have been verified with experiments with satisfied agreement.

Furthermore, NSGA-II (Non-dominated Sorting Genetic Algorithm-II) is selected for global optimization of the swept and anhedral combination rotor configuration. Kriging method and Optimal Latin Hypercube-Sampling (Opt-LHS) method are employed to build an effective surrogate model. Optimization point adding method is introduced in the process of building Kriging model to improves the fitting accuracy. The optimal result shows that the maximum figure of merit is increased by 17.5% with a 1.915dB reduction in OASPL under the constraints, which verifies the effectiveness of the MDO method developed in this paper. It also indicates that the shape of the blade tip has a significant impact on the performance of the rotor.

Keywords: Rotor wing, Aerodynamic, Aeroacoustics, Multidisciplinary, Optimization

1 Introduction

Compared to fixed wing aircraft, helicopters have advantages of vertical takeoff and landing, hovering, and high maneuverability. The rotor, as the provider of both lift and the control surface, is the technical core of helicopter development. The performance of rotor blades directly affects the flying qualities, reliability and safety of helicopters[1]. However, unlike the steady flow environment of a fixed wing aircraft, the rotor blade section inlet flow velocity has obvious unsteady characteristics. The variable inflow makes the flow field and aerodynamic characteristics of the rotor very complex. In the tip region, problems such as shock waves, stalls and tip vortices are prominent, which presents a great challenge to rotor design.

Conventional rotor aerodynamic design is mainly aimed at rotor aerodynamic performance, researching on airfoil configuration and blade twist distribution design. However, the previous blade element theory and vortex theory are difficult to analyze the aerodynamic characteristics of rotors from the flow details [2]. In order to adapt to the requirements of new blade tips and new rotors configuration, applications of CFD methods develop rapidly. Modern helicopter advanced design tends to combine CFD methods with numerical optimization algorithms. By parametrizing the rotor configuration, the optimal rotor shape that meets aerodynamic performance, noise levels and other objectives is designed.

Early rotor optimization mainly focused on the single objective of aerodynamic performance, involving a relatively small number of optimization variables. With the application of surrogate models, rotor optimization technology has developed into multidisciplinary research involving aerodynamics, aeroacoustics, and elastic mechanics. A comprehensive optimization algorithm based on Neural Network model is developed by LaMarsh et al. [3], which selects the parameters of rotor blade twist distribution, root chord length, taper ratio, and taper starting position, aiming to reduce the required power for hover and forward flight state. A genetic algorithm based on the Kriging surrogate model is applied for design of rotor airfoils by Wang Q and Zhao Q-J [4], in order to obtain airfoils with better aerodynamic performance.

Although research of the blade shape design effect on rotor aerodynamic performance has matured, the mechanism of suppressing noise has not been clearly revealed, which is related to the complex flight conditions of helicopters. The noise characteristics of rotors are closely related to the flow field and aerodynamic characteristics of rotors. The aerodynamic optimization and noise reduction research

of rotors have different design goals and constraints, while they are also coupled and affect each other[5].

High speed silent helicopters are the current development direction of helicopter technology, and passive suppression of rotor aerodynamic noise is an important core technology in this field. The tip area of the blade is the main noise source. In recent years, blade tip design has been extensively studied internationally. The effects of blade tip thickness, sweep angle, and taper ratio on high-speed pulse (HSI) noise are analyzed by Aoyama et al. [6]. The study found that the strength, position, and supersonic range of shock waves on the blade surface determine the magnitude of HSI noise; The taper tip design can effectively reduce HSI noise, and the swept back tip design can make the shock wave position moving towards the blade tip. Shi Y-J's research [7] shows that the swept forward tip design can increase the interference angle on the advancing blade, making it tends to the oblique interference, which reducing the blade-vortex interference (BVI) noise; The taper tip design reduces the pulse load caused by BVI and effectively decreases thickness noise by reducing the blade tip area; The anhedral tip design can suppress BVI noise by increasing the vertical interference distance between tip vortex and the rear blade. Moreover, BERP blades[8], Neta Tip blades[9], and Blue Edge blades[10], have been successfully applied to multiple helicopter models such as the Lynx, Black Hawk, and Eurocopter. Their payload and figure of merit are improved, with noise reduction by 3-4 dB.

Genetic Algorithm is an optimization algorithm with strong global search ability. However, it requires frequent calls to CFD during iteration, resulting in huge computational costs. In order to improve optimization efficiency, the solution is to use a suitable surrogate model while considering the hovering flow field of the rotor as quasi-steady, and to solve it using MRF (Moving Reference Frame) method[11]. Meanwhile, when the speed of the rotor tip in hover is less than 0.7 Ma, the noise is mainly composed of linear noise including thickness noise and loading noise, while the influence of quadrupole noise is relatively small[12]. Therefore, the aerodynamic calculation results of the quasi-steady flow field can be used to obtain the linear noise, which greatly improves computational efficiency while ensuring computational accuracy.

In this paper, firstly theoretical formulas for aerodynamic and noise performance calculation are presented, and then a numerical model is constructed to predict the aerodynamic and noise performance of the rotor, compared with experimental results to verify its accuracy. Next, a parameterized optimization design method for blade

shape is established, and aerodynamic and noise optimization objectives and constraints are constructed to obtain optimization results. Finally, the performance of the blade before and after optimization is compared through numerical simulation.

2 Rotor Aerodynamic and Acoustic Performance Calculation

2.1 Aerodynamic Performance

In hover state，the main rotor torque coefficient (C_Q) , thrust coefficient (C_T) and figure of merit (FM) are used to evaluate rotor performance, see the equations (2-1)~(2-3).

$$C_Q = \frac{Q}{\rho\pi R^2(\Omega R)^2 R} \tag{2-1}$$

$$C_T = \frac{T}{\rho\pi R^2(\Omega R)^2} \tag{2-2}$$

$$FM = \frac{C_T^{3/2}}{\sqrt{2}C_Q} \tag{2-3}$$

Where T is the thrust, Q is the torque, Ω is the Rotor speed, R is the rotor radius , ρ is the air density.

2.2 Acoustic Performance

Noise Equation

This paper employed the FW-H equation to specify the sound generation equation of the control surface moving arbitrarily in the fluid field[13], see equation (2-4):

$$\begin{aligned}\left(\frac{1}{c^2}\frac{\partial^2}{\partial t^2}-\frac{\partial^2}{\partial {x_i}^2}\right)p'(x_i,t) = &\frac{\bar{\partial}}{\partial t}\{[\rho_\infty v_n+\rho(u_n-v_n)]\delta(g)\}\\ &-\frac{\bar{\partial}}{\partial x_i}\{[-\boldsymbol{P'}_{ij}\cdot\boldsymbol{n'}_j+\rho\boldsymbol{u}_i(u_n-v_n)]\delta(g)\}\\ &+\frac{\bar{\partial}^2}{\partial x_i x_j}[(-\boldsymbol{P'}_{ij}+\rho\boldsymbol{u}_i\boldsymbol{u}_j-c^2\rho'\delta_{ij})\cdot H(g)]\end{aligned} \tag{2-4}$$

Where c, $\boldsymbol{u}_i$ and $\boldsymbol{u}_j$, $\boldsymbol{P'}_{ij}$ are the sound velocity, velocity components, and stress tensor, respectively. $p'(x_i,t)$ is the sound pressure intensity value of the observation point x_i at time t. δ_{ij} is Kronecker symbol. The subscript "∞" represents the undisturbed item, the superscript "$'$" represents the disturbed item. The subscript "n" represents the projection in the normal direction outside the control surface. $\bar{\partial}$ is the generalized derivative, $H(g)$ is the Heaviside function, and $\delta(g)$ is the Dirac function.

For the unsteady flow of rotors, the non-rotating interface is selected as the

penetrable sound source surface, the thickness noise, loading noise, and quadrupole noise can be calculated（see Fig. 3-5 in the following text）. For the quasi-steady flow of the rotor, the blade surface is selected as the impenetrable sound source surface, only the thickness noise and loading noise can be considered (see Fig. 3-3).

Using Fast Fourier Transform (FFT), the Sound Pressure Level (SPL) can be calculated in equation (2-5)

$$L_p = 10lg\left(\frac{\tilde{p}}{p_{ref}}\right)^2 = 20lg\left(\frac{\tilde{p}}{p_{ref}}\right) \tag{2-5}$$

Where L_p is SPL, which is measured in decibels (dB); $\tilde{p}$ is sound pressure, and $p_{ref} = 2 \times 10^{-5}$Pa.

It is common to define sound harmonics representing the human ear sensitivity through the A-weighted Sound Pressure Level (ASPL)[14].

$$L_A = L_p + \Delta L_A \tag{2-6}$$

$$\Delta L_A = \frac{12200^2 f^4}{(f^2 + 20.6^2)(f^2 + 12200^2)\sqrt{f^2 + 107.7^2}\sqrt{f^2 + 737.9^2}} \tag{2-7}$$

Where *f* is frequency.

The A-weighted total sound pressure level (OASPL) can be expressed as:

$$OASPL = 10lg\left(10^{\frac{L_{A1}}{10}} + 10^{\frac{L_{A2}}{10}} + \cdots + 10^{\frac{L_{An}}{10}}\right) \tag{2-8}$$

Where L_{Ai} represents the nth A-weighted sound pressure level calculated from equations (2-6).

3 Simulation Models of Rotor Aerodynamic and Acoustic Performance

3.1 Parameters of Original Blades

The original rotor blade is designed according to the Blue-Edge blade with double-swept and anhedral configuration[15], as shown in Fig.3-1. The parameters and working conditions are shown in the Table 3-1.

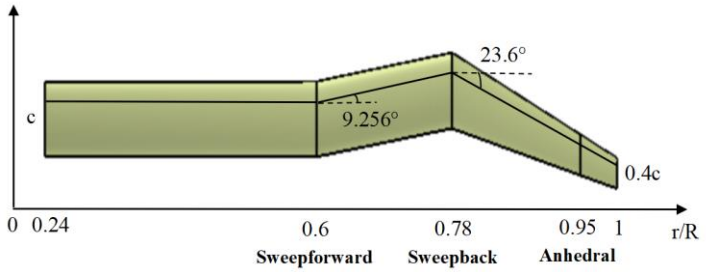

Figure 3-1. Model rotor blade geometric configuration

Table 3-1. Model blade parameters and working conditions

Airfoil	OA213	Number of blades	4
Radius	750mm	Aspect ratio	13
Taper ratio	0.4	Chord length at 0.24~0.78R	57.7mm
Sweepforward position	450mm	Sweepforward angle	9.256°
Sweepback position	585mm	Sweepback angle	23.6°
Anhedral position	712.5mm	Anhedral angle	15.0°
Root position	180mm	Twist angle(0~R)	-10°
Collective pitch	5°~ 12°	Rotating speed	1300rpm

3.2 Experimental Results of the Original Rotor

The rotor was made of carbon fiber composite materials manufactured by Anyang Haoke Aviation Technology Co., Ltd in China. The hovering test of the rotor was carried out in the anechoic chamber of FL-52 wind tunnel of AVIC Aerodynamics Research Institute in China, shown in Fig. 3-2. The ambient temperature for measurement is 21.8℃, the atmospheric pressure is 99599Pa, and the relative humidity is 32.7%.

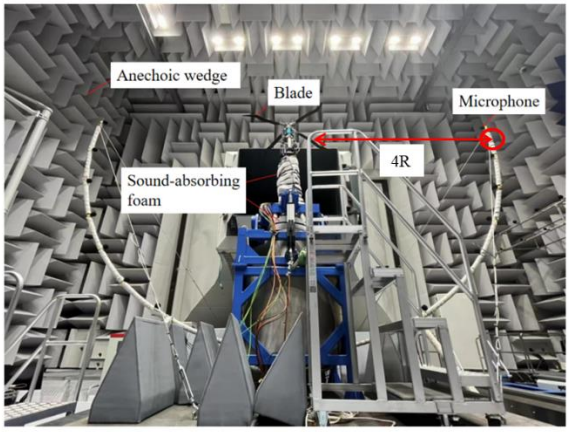

Figure 3-2. Original rotor in test

Both the collective pitch and periodic pitch of the rotor are controlled by the rig. It is equipped with thrust and torque balance to measure aerodynamic force. The range of the thrust balance is 700N, and the accuracy range is 0.019% FS. The torque measurement adopts the T22/20N · m dynamic sensor from German HBM company, with a range of 20N · m and a measurement accuracy of 0.02% FS. The rotating speed is in range 1100~1400rpm, which has an accuracy of 0.1%.

The noise observation point is located at 4R from the center of the rotor disc. The muffler used in noise measurement is Danish BK sound sensor. The signal-to-noise ratio in the anechoic chamber is good enough to ignore background noise. The microphones are symmetrically arranged every 10 ° on each side of the array frame with a radius of 3m. The sampling time for noise data is 10s, the noise resolution is 1Hz, the analysis bandwidth is 20kHz, and the sampling rate for sound pressure data signals is 40.96kHz. Measuring results are presented in Fig. 3-4 and Table 3-2.

3.3 Aerodynamic Performance Simulation and Results Validation

The quasi-steady flow simulation is employed to predict the aerodynamic performance of rotor in hover by the discretization of N-S equation using software Star CCM+, where periodic boundary condition is applied, as shown in Fig. 3-3. The unstructured meshes are created for static domain and rotating domain separately. This model is aimed to reduce calculation cycle and works with automatic optimization algorithm. the total number of grids is 1.3 million. In the simulation model, the third-order MUSCL scheme is adopted for space discretization. The K- ω SST turbulence model is employed. No-slip and free-inflow boundary condition are

selected at blade surface and far field respectively. The blade is set as non-slip wall and impermeable sound source surface.

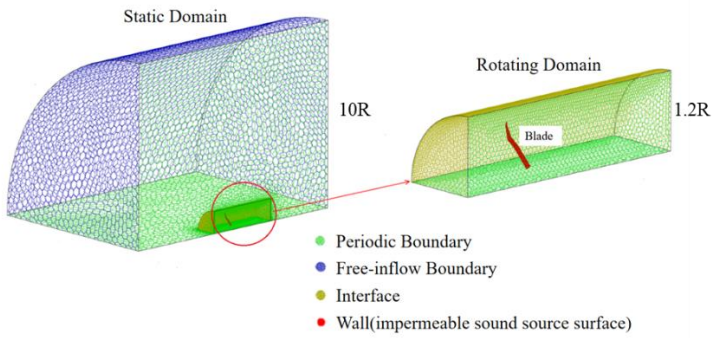

Figure 3-3. Boundary conditions for quasi-steady flow simulation

Thrust coefficient， torque coefficient and figure of merit predicted by the numerical method are compared with experimental data in Fig. 3-4 at rotor speed of 1300 rpm for collective pitch range 5~15°. The maximum collective pitch of the experiment is 12°due to torque balance approaching maximum range value.

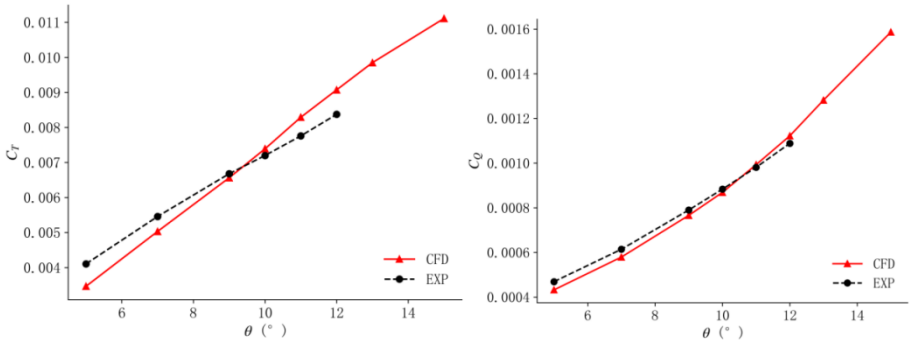

(a)Comparison of thrust coefficient (b)Comparison of torque coefficient

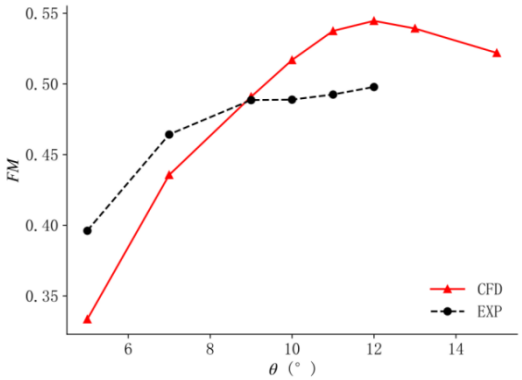

(c)Comparison of figure of merit

Figure 3-4. Comparison between CFD results and EXP data at 1300 rpm

It can be seen from Fig. 3-4 that both methods indicate same trend of C_T and C_Q increasing with θ, and FM reaches its maximum at $\theta = 12°$. The simulation errors of CFD result for C_T, C_Q and FM are$-15.6\% \sim 8.3\%$, $-7.8\% \sim 3.1\%$ and$-15.8\% \sim 9.4\%$, respectively. The analysis of the error reasons is as follows: Firstly, using a fully turbulent model in CFD will result in a smaller calculated value of rotor thrust and a larger calculated value of torque; Secondly, in the experiment, the rotor exhibits flapping motion with a cone angle of around 3-5 degrees, while CFD does not consider it; Thirdly, the experimental platform has interference with the hovering flow field. In summary, the comparison of CFD results with experimental data demonstrates that the CFD method has good accuracy for aerodynamic performance prediction of rotor in hover.

Furthermore, the original blades show a good performance at collective pitch 12 ° in experiment, which will be used as the designed working condition for shape optimization.

3.4 Aeroacoustic Performance Simulation and Results Validation

For the quasi-steady model, taking the rotor blade as the sound source, only the thickness and load noise are considered. The calculated OASPL of the CFD result at the noise observation point shown in Fig. 3-2 is compared with experimental data in Table 3-2. For the unsteady model, the 4 blades are simulated with sliding mesh technology. In Fig. 3-5, the non-rotating interface of the cylindrical surface in the outside of the stationary domain is selected as the penetrable sound source surface to capture the nonlinear harmonic noise，i.e. the quadrupole noise in subsonic flow.

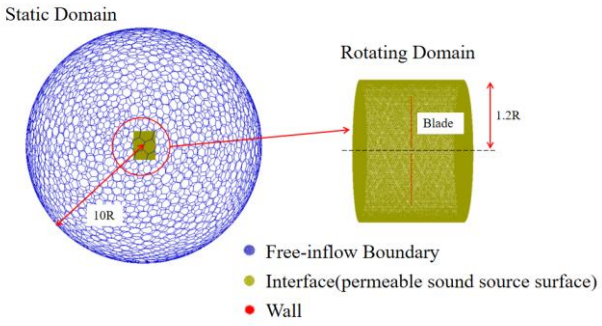

Figure 3-5. Boundary conditions for unsteady flow simulation

The total numbers of grids of the rotating domain and the stationary domain unsteady are 10.2 million and 2.4 million separately, resulting in whole grid number 12.6 million. To increase the accuracy and reduce flow dissipation, The third-order MUSCL scheme is adopted for space discretization, and the second-order implicit LU-SGS scheme is adopted for time discretization. The IDDES model for turbulent flow is employed to capture flow details. Time step for relative blade rotation of 0.5° is selected. The aerodynamic and aeroacoustic results under working condition of θ =12° are provided together in Table 3-2.

Table 3-2. Comparison among experiment data, quasi-steady result and unsteady result

θ=12°	C_T	C_Q	FM	OASPL (dB)
EXP	0.008376	0.001089	0.4979	67.8
CFD (quasi-steady)	0.008757	0.001042	0.5561	63.5
Error	4.5%	-4.3%	11.7%	-4.3
CFD (unsteady)	0.00860	0.001062	0.5309	69.2
Error	2.7%	-2.4%	6.6%	1.4

The error of quasi-steady flow field noise is -4.3dB. The reason for the error is that only thickness noise and load noise are calculated in the quasi-steady flow field, and the quadrupole noise is ignored. In the unsteady flow, tip vortex and rotor wake are simulated which are ignored in the quasi-steady flow model. The FW-H equation based on penetrable surface is used to calculate and the rotor noise including the quadrupole noise. Its error is relatively small, which is 1.4dB, indicating the unsteady noise calculation method is more reliable.

Considering that the quasi-steady flow model can provide an accurate aerodynamic performance and primary acoustics performance of the rotor with a short

calculation period, which only costs $1/480$ of the unsteady computation time, it is quite suitable for optimization iteration. Therefore, the optimal shape design of the blade is built on the quasi-steady model, and the final simulation result are provided by the unsteady model as a modification.

4 Optimization Scheme

The optimal Latin hypercube (Opt-LHS) method[16] is used to generate initial sample points. Kriging model[17] is applied to replace the response value in the design space. Multi-objective genetic algorithm NSGA-II[18] is selected to find the approximate Pareto frontier in the design space, and the Pareto solution is added to the sample point set as new sample points to update the Kriging model.

4.1 Design Variables

There are 9 design variables selected to uniquely determine the plane shape of the rotor blade as shown in Table 4-1.

Table 4-1. Optimize design variables and their value ranges

Variable name	Original value	Value range
Sweepforward angle	9.256°	5°~ 15°
Sweepback angle	23.6°	18°~ 28°
Anhedral angle	15°	10°~ 20°
Collective pitch	12°	5°~ 16°
Sweepforward position	450mm	445mm ~ 455mm
Sweepback position	585mm	580mm ~ 590mm
Chord length (0.24~0.78R）	57.7mm	53mm ~ 63mm
Taper ratio	0.4	0.2 ~ 0.7
Twist angle(0~R)	-10°	-12° ~ -8°

4.2 Optimization Goals and Constraints

Two optimization design objectives are considered: the highest FM and minimum OASPL at the observation point. Constraints includes C_T and C_Q within a 5% variation range. The mathematical description of this optimization problem is shown in Equation (4-1):

$$\begin{aligned} &\text{Objective: Max: } FM \\ &\qquad\quad \text{Min: } OASPL \\ &\text{s.t.: } \ 0.95C_{T_0} < C_T < 1.05C_{T_0} \\ &\qquad 0.95C_{Q_0} < C_Q < 1.05C_{Q_0} \end{aligned} \tag{4-1}$$

4.3 Optimization Process

In this paper, NSGA-II is adopted as the optimization method, considering the global optimization characteristics without difficulty to be stuck at locally optimal value. However, the convergence speed of the algorithm is generally slow and the CFD solver will be invoked frequently in the calculation process, which makes the calculation time increase sharply. Therefore, Kriging Surrogate model is employed to replace the complex and time-consuming iterative work. The optimization design steps are as follows:

1) There are 91 initial sample points extracted using Opt-LHS method and their response values are calculated;

2) A Kriging model is established on the quasi-steady flow model.

3) The NSGA-II algorithm is employed to find the sample points corresponding to the Pareto frontier;

4) The numerical simulation module is invoked to solve the objective function of the sample points obtained in step 3, with automatic generation of grids and calculation;

5) The program will terminate if the stop criteria are met; otherwise, it will continue;

6) The sample points will be filled and updated in the Kriging model. Then the procedure will return to step 2.

The procedure is shown in Fig. 4-1.

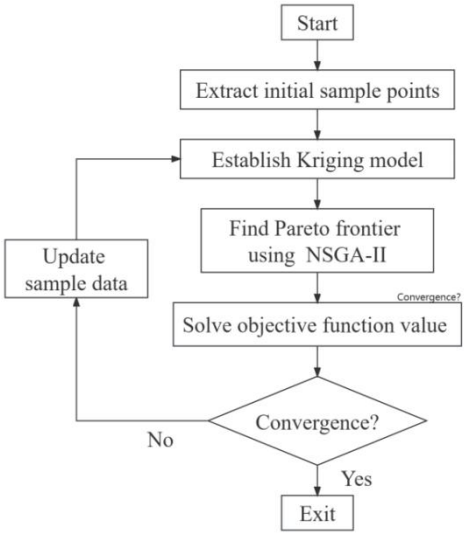

Figure 4-1. Optimization process flowchart

5 Optimization Results

After 6 optimization cycles, a total of 150 blade shapes are calculated and Pareto frontier containing 10 optimal solutions is obtained, as shown in Fig. 5-1. It can be seen that the two objective function values of all Pareto-optimal points are better than the original shape.

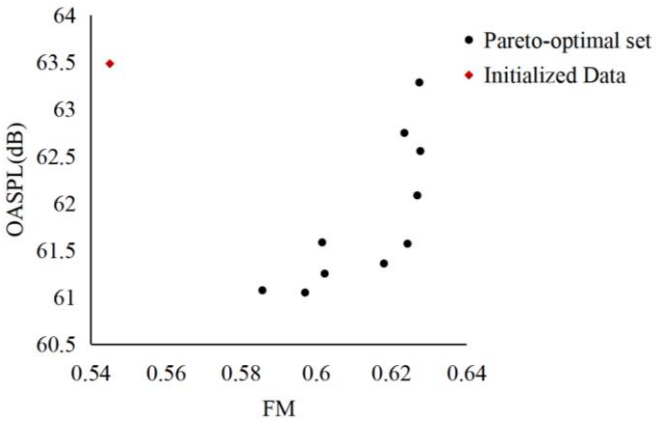

Figure 5-1. Pareto solution set obtained from multi-objective optimization design

Table 5-1 shows the change of objective function at FM maximum point and the

fitting error of Kriging model in the process of optimization design. It can be seen that as the number of cycles increases, more and more sample points are added to the sample set, and the fitting accuracy of the Kriging model has also been greatly improved. The fitting error decreases from 6.75% to 0.91%.

Table 5-1. Changes in objective function and fitting error

Number of cycles	FM Kriging value	FM CFD value	Error
1	0.658482008	0.616864863	6.75%
2	0.653337156	0.618989855	5.54%
3	0.641216359	0.62374347	2.80%
4	0.637130476	0.623386778	2.20%
5	0.632157061	0.623482907	1.39%
6	0.629891345	0.624221715	0.91%

A point of Pareto-optimal set in Fig. 5-1 is selected as the final optimal solution and compared with the original blade. Fig. 5-2 shows a comparison of blade geometry and Table 5-2 shows the comparison of design variables. After optimization, the sweep angles and anhedral angle decrease, the chord length increases, resulting in the trend of becoming a straight blade with smaller aspect ratio in the middle and lower parts of the blade. The taper ratio is decreased which may results in weak tip vortex The variation of sweep positions and twist angle is relatively small. The optimum working condition changes to $\theta = 11°$.

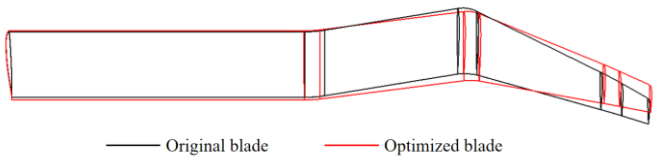

Figure 5-2. Comparison of blade geometry before and after optimization

Table 5-2. Comparison of design variables before and after optimization

Variable name	Original value	Optimal value
Sweepforward angle	9.256°	7.23° ↓

Sweepback angle	23.6°	19.26° ↓
Anhedral angle	15°	10.24° ↓
Collective pitch	12°	11° ↓
Sweepforward position	450mm	447.42mm ↑
Sweepback position	585mm	588.58mm ↑
Chord length (0.24~0.78R）	57.7mm	60.87mm ↑
Taper ratio	0.4	0.3032 ↓
Twist angle(0~R)	-10°	-10.32° ↑

Fig. 5-3 shows a comparison of upper surface pressure distribution before and after the optimization. For both blades, the low-pressure region mainly gathers in the backswept and anhedral sections of them and pressure changes significantly in chord-wise direction. Compared to the original blade, the optimized blade has a larger pressure gradient, a larger low-pressure area, and a smaller high-pressure area.

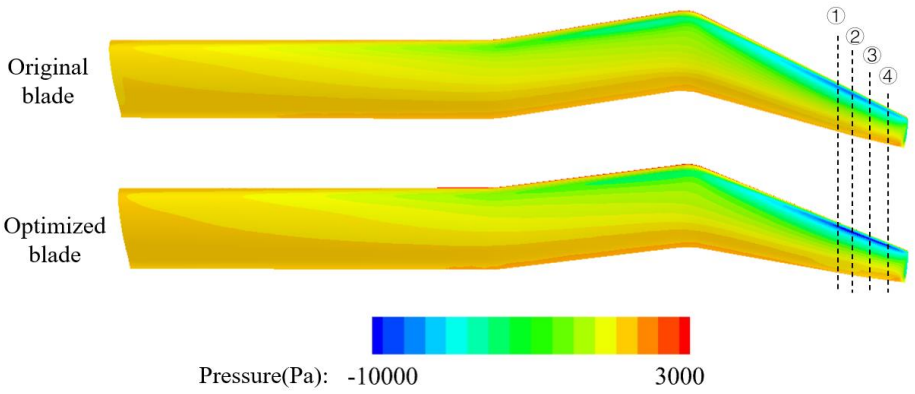

Figure 5-3. Comparison of pressure distribution on blade surface(Pa)

Four spanwise cross-sections at tip region are selected as shown in Fig. 5-3, with $r/R = 0.92, 0.94, 0.96, 0.98$, respectively. Fig. 5-4 shows the pressure comparison at each cross-section, and it can be seen that the optimized blade has a higher negative pressure value, resulting in greater lift.

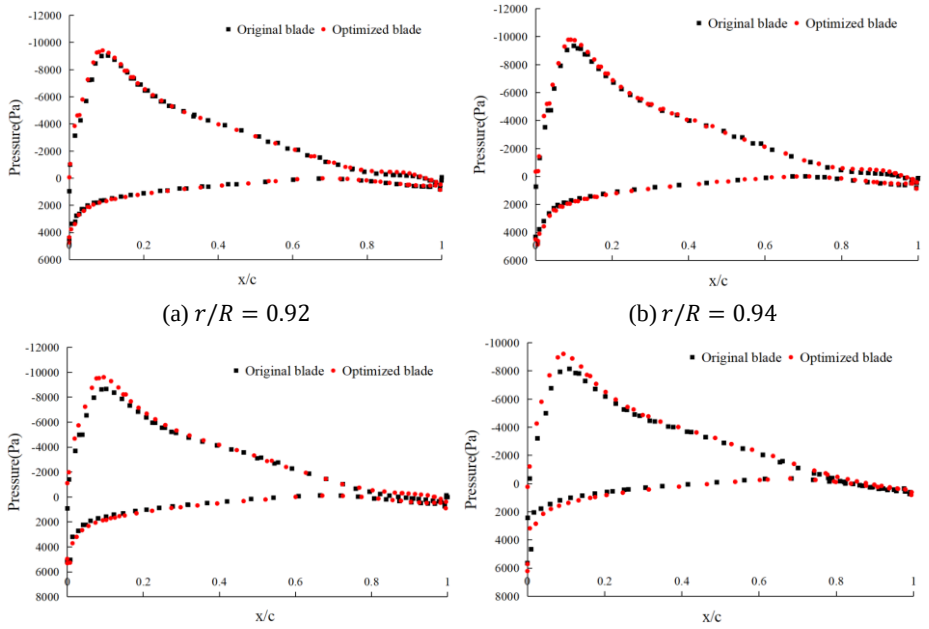

(a) $r/R = 0.92$ (b) $r/R = 0.94$

(c) $r/R = 0.96$ (d) $r/R = 0.98$

Figure 5-3. Comparison of pressure at different spanwise cross-section

In order to compare the integral performance of the rotors in various collective pitch, Fig. 5-3 shows the aerodynamic performance between the original blade and the optimized blade under different collective pitches. As can be seen that for all pitch range, C_T of the optimized blade increases at different θ, while C_Q varies slightly. The overall FM is better than the original blade. The maximum FM increased by 17.5%.

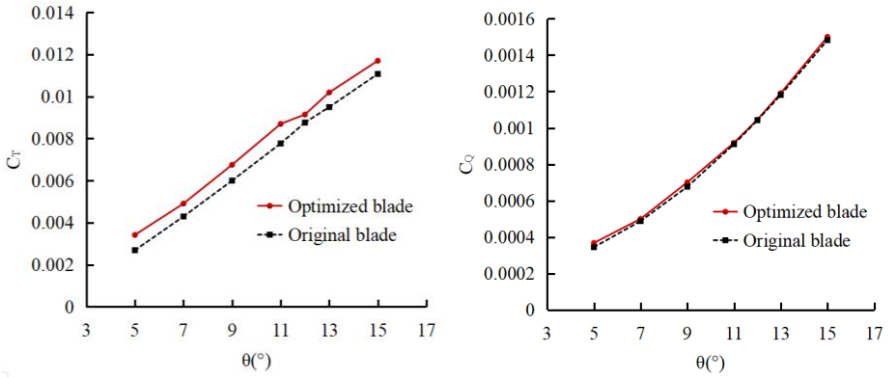

(a)Comparison of thrust coefficient (b)Comparison of torque coefficient

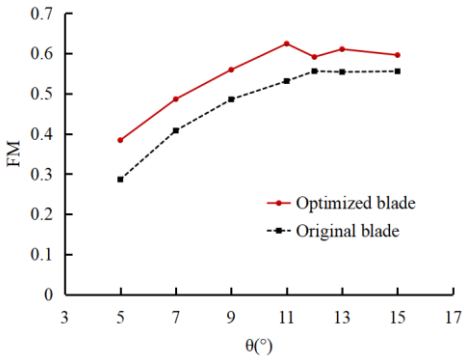

(c)Comparison of figure of merit

Figure 5-3. Comparison the original blade and the optimal blade at 1300 rpm

The optimal blade acoustic performance was calculated by the unsteady flow model at collective pitch 11°. Fig. 5-4 shows the noise comparison in time-domain between the original blade and the optimal blade at θ corresponding to maximum FM. It reveals a smaller distance between peak and trough for the optimized rotor. The negative peak sound pressure is reduced by 21.3%, and OASPL is reduced by 1.915dB as shown in Table 5-3.

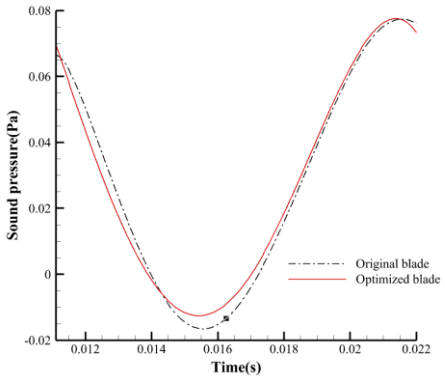

Figure 5-4. Noise comparison in time-domain

Table 5-3. Noise comparison between the original blade and the optimal blade

	Original blade	Optimized blade	Reduction
Negative peak sound pressure(Pa)	-0.0228	-0.0179	21.3%

OASPL(dB)	63.5	61.6	1.9

6 Conclusions

1）The quasi-steady and unsteady flow simulation and acoustic prediction are established for the rotor wing in hover, result shows that: Compared to the wind tunnel test at $\theta = 12°$, the FM errors are 11.8% for quasi-steady flow and 6.6% for unsteady flow, and the OASPL errors are -4.3dB for quasi-steady flow and 1.4dB for unsteady flow. The quasi-steady flow model can provide an accurate aerodynamic performance and primary acoustics performance of the rotor with a significantly faster calculation speed.

2）An optimal design method is established for comprehensive optimization of aerodynamic and noise performance of rotor blade. Nine blade geometry parameters are selected as the design variables. Figure of merit and OASPL are chosen as optimization objective, with C_T and C_Q as constraints. The NSGA-II optimization method based on Surrogate model is adopted, and the optimization point adding method is introduced in the process of building Kriging model, which highly improves the fitting accuracy. Pareto-optimal solution set with improved aerodynamic and noise performance and satisfying all constraints are obtained.

3）Compared with the original blade, the optimized blade has improved the thrust coefficient at different collective pitches, and the figure of merit has been significantly improved, with a maximum improvement value of 17.5%. Also, the optimized blade has improved the noise performance. The negative peak sound pressure is reduced by 21.3%, and OASPL is reduced by 1.9 dB.

7 Acknowledgments

This work was supported by the National Key Laboratory of Science and Technology on Aerodynamic Design and Research (20210301-3).

References

[1] Zhang C-L. Development of Helicopter Rotor Technology[N], China Aviation News, 2000.

[2] Zhao Q-J, Zhao G-Q, Wang Q, et al. Advanced Rotor design Aerodynamics[M]. Beijing: Science Press, 2020.

[3] Lamarsh I W, Walsh J, Rogers J. Aerodynamic performance optimization of a rotor blade using a neuralnetwork as the analysis[C]. 4th Symposium on Multidisciplinary Analysis and Optimization, 1992.
[4] Wang Q, Zhao Q-J. Synthetical optimization design of rotor airfoil by genetic algorithm[J]. Journal of Aerospace Power, 2016, 31(6): 1486-1495.
[5] Shi Y-J, Xu G-H, Zhao Q-J.Helicopter Aeroacoustics[M]. Beijing: Science Press, 2019:133-134.
[6] Aoki M, Kondo N, Saito S, et al. Effect of blade-tip shape on high-speed rotor noise[C/OL]. 14th Applied Aerodynamics Conference. New Orleans,LA,U.S.A.: American Institute of Aeronautics and Astronautics, 1996.
[7] Shi Y-J. Research on Aerodynamic and Noise Characteristics of Helicopter Rotor-Vortex Interaction Based on CFD Method [D]. Nanjing University of Aeronautics and Astronautics, 2010.
[8] Brocklehurst A, Duque E. Experimental and numerical study of the British experimental rotor programme blade[C]. Flight Simulation Technologies Conference and Exhibit. 1990: 3008.
[9] Leoni R D. Black Hawk: The Story of a World Class Helicopter[M]. Reston: America institute of Aeronautics and Astronautics. 2007.
[10] Rauch P, Gervais M, Cranga P, et al. Blue edge; the design, development and testing of a new blade concept[C]. Virginia: Proceedings of the 67th Annual Forum of the American Helicopter Society, 2011.
[11] Han Z-H, Song W-P, Qiao Z-D. Aeroacoustic Calculation for Helicopter Rotor in Hover and inForward Flight Based on FW-H Equation[J]. Chinese Journal of Aeronautics, 2003, 24(5): 400-404.
[12] Shi Y-J, Xu G-H, Zhao Q-J. Helicopter Aeroacoustics[M]. Beijing: Science Press, 2019.
[13] Ffowcs Williams J E, Hawkings D L. Sound Generated by Turbulence and Surfaces in Arbitrary Motionp[J]. Philosophical Transactions of the Royal Society. 1969，A264(1151) : 321-342.
[14] Bennett R L, Pearsons K S. Handbook of aircraft noise metrics[R]. Washington: National Technical Information Service, N8121871, 1981.
[15] Kang M-H, Zhao X, Yao R, et al. Influence of tip dihedral on rotor aerodynamic performance and tip vortex[R]. 33rd ICAS,2022.
[16] Giunta A A, Wojtkiewicz S F, Eldred M S, et al. Overview of modern design of experiments methods for computational simulations[J]. AIAA-2003-649, 2003.

[17] Jeong S, Murayama M, Yamamoto K. Efficient optimization design method using Kriging model[J]. AIAA-2004-118, 2004.
[18] Deb K，A Fast and Elitist Multiobjective Genetic Algorithm: NSGA-II［J］. IEEE Transaction on Evolutionary Computation，2002，6(2) : 182-197. doi: 10.1109 /4235.996017．